NANO LETTERS

Letter

pubs.acs.org/NanoLett

Eleven Nanometer Alignment Precision of a Plasmonic Nanoantenna with a Self-Assembled GaAs Quantum Dot

Markus Pfeiffer,[†,‡] Klas Lindfors,[†,‡] Hongyi Zhang,[†,‡] Bernhard Fenk,[†] Fritz Phillipp,[§] Paola Atkinson,[∥] Armando Rastelli,[∥] Oliver G. Schmidt,[∥] Harald Giessen,[‡] and Markus Lippitz*[,†,‡]

[†]Max Planck Institute for Solid State Research, Heisenbergstrasse 1, D-70569 Stuttgart, Germany

[‡]Fourth Physics Institute and Research Center SCOPE, University of Stuttgart, Pfaffenwaldring 57, D-70550 Stuttgart, Germany

[§]Stuttgart Center for Electron Microscopy, Max Planck Institute for Intelligent Systems, Heisenbergstr. 3, D-70569 Stuttgart, Germany

[∥]Institute for Integrative Nanosciences, IFW Dresden, Helmholtzstrasse 20, D-01069 Dresden, Germany

Supporting Information

ABSTRACT: Plasmonics offers the opportunity of tailoring the interaction of light with single quantum emitters. However, the strong field localization of plasmons requires spatial fabrication accuracy far beyond what is required for other nanophotonic technologies. Furthermore, this accuracy has to be achieved across different fabrication processes to combine quantum emitters and plasmonics. We demonstrate a solution to this critical problem by controlled positioning of plasmonic nanoantennas with an accuracy of 11 nm next to single self-assembled GaAs semiconductor quantum dots, whose position can be determined with nanometer precision. These dots do not suffer from blinking or bleaching or from random orientation of the transition dipole moment as colloidal nanocrystals do. Our method introduces flexible fabrication of arbitrary nanostructures coupled to single-photon sources in a controllable and scalable fashion.

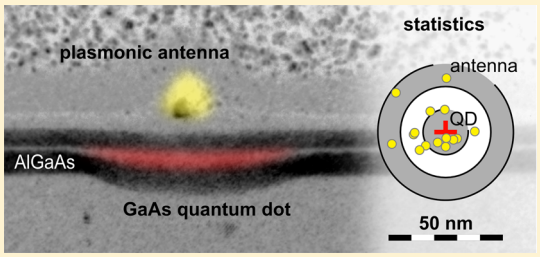

KEYWORDS: *Plasmon−exciton coupling, optical antennas, self-assembled quantum dots, nanopositioning*

Realizing a single photon transistor is the holy grail of nanophotonics.[1,2] To reach this goal, the interaction of single quantum emitters and dielectric and plasmon resonant metallic nanostructures is under intense study.[3−5] Some of the milestones of this work are optical nonlinearities on the single-photon level,[6−8] enhanced spontaneous emission into free space with plasmonic structures,[9−12] as well as unidirectional single photon emission from an optical antenna excited by a single colloidal nanocrystal.[13] The quality of such devices depends critically on the ability to position and orient the structures with respect to the quantum emitter.[2,14] In plasmonics, the majority of studies on coupling single quantum emitters to optical nanostructures have dealt with organic molecules or colloidal nanocrystals as emitters,[9−13] which suffer severely from blinking and bleaching. For these, wet chemical[15,16] or scanning probe techniques[17,18] can be used to position and align the two components of the hybrid structure to realize simple plasmonic devices. For self-assembled quantum dots and structures with more than one emitter, these approaches are in general not applicable. Overcoming this limitation would allow the use of bright and stable self-assembled quantum dots in nanoscale plasmonic structures. Here, we demonstrate the fabrication technique that successfully meets this challenge and apply our method to couple single self-assembled quantum dots to plasmonic nanoantennas.

The best reported positioning accuracy so far for self-assembled semiconductor quantum dots in a nanostructure is on the order of several tens of nanometers.[19−22] However, for plasmonic structures the required accuracy is on the nanometer scale, as plasmonic fields decay on a length scale much shorter than the wavelength. As an example, Figure 1 shows the calculated enhancement of the electric field in the vicinity of a plasmonic nanoantenna driven on its resonance. The antenna modifies the otherwise constant field distribution in the semiconductor substrate on a 10 nm length scale. This length scale defines the demand on accuracy in positioning quantum emitters in plasmonic structures.

The novel ingredient in our method (Figure 2) resulting in high positioning accuracy is the use of single nonblinking and stable semiconductor quantum dots whose position we can determine by imaging the sample using scanning electron microscopy (SEM). Combined with a nanofabrication process, which allows reproducible and aligned multilayer structures, this results in an alignment accuracy on the 10 nm scale. Our quantum emitters are low-density self-assembled GaAs quantum dots in AlGaAs barriers grown by MBE (for details on sample growth see Supporting Information). In these

Received: October 7, 2013
Revised: December 6, 2013
Published: December 16, 2013

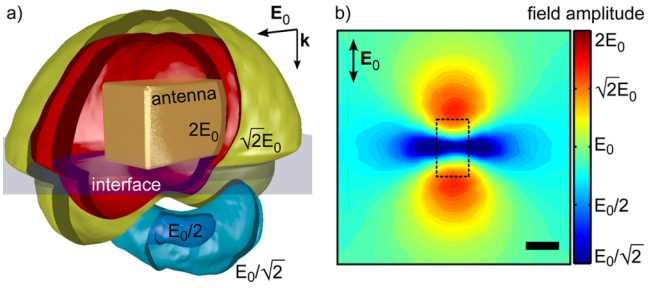

Figure 1. Variation of the electromagnetic field by a plasmonic nanostructure. (a) Isosurfaces of field enhancement and reduction for a plane wave (wavelength 738 nm, wave vector **k**, and amplitude $\mathbf{E}_0$) impinging on a gold nanoantenna ($20 \times 20 \times 35$ nm^3) on a substrate (n = 3.5). The value of the field amplitude is indicated close to each isosurface. (b) Field amplitude in a plane 20 nm beneath the sample surface in which quantum emitters could be positioned (scale bar 20 nm). The field varies significantly on a nanometer length scale. This defines the requirements on positioning accuracy of the antenna relative to the quantum emitters. The outline of the antenna is shown with the dashed black line. Details on the simulation can be found in the Supporting Information.

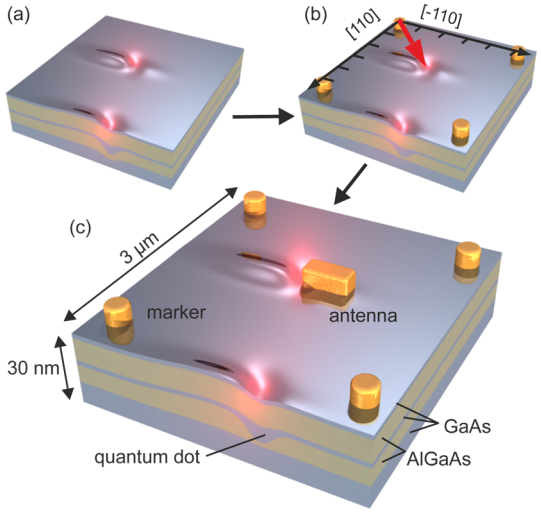

Figure 2. Key steps of our fabrication method. (a) Single self-assembled GaAs quantum dots, whose position is visible on the sample surface as characteristic topography features. (b) A coordinate system is defined by a grid of gold markers. It allows us to record the position of the quantum dot. (c) In a second, aligned nanofabrication step a plasmonic nanoantenna is positioned next to the quantum dot. In this sketch, the quantum dot and antenna are drawn with the same in-plane scale. In reality, the markers are further apart. The height of the quantum dot feature is exaggerated.

samples, a characteristic surface topography feature signals the position of each quantum dot (Figure 2a).[23,24] This feature, consisting of an elongated bump with an elliptically shaped depression at one end, allows determination of the position of the quantum emitter with nanometer precision using SEM. SEM is well-suited to determine the relative position of objects with high precision due to its resolution and short exposure times on the order of a few seconds. The quantum dot is located beneath the surface depression at a depth determined by the thickness of the top barrier layer. In the samples used here the burial depth is 18 nm. The quantum dot has two energetically almost degenerate exciton transitions with mutually orthogonal transition dipole moments oriented along specific crystal directions. Knowing the precise position of the quantum dots allows us to use nanofabrication methods to position plasmonic structures in a controllable and scalable fashion. First a grid of markers is patterned on the sample surface using electron beam lithography. The marker grid can be aligned with the semiconductor crystal axes with high precision using cleaved sample edges. The positions of selected quantum dots are then determined with respect to the marker grid using the surface topography feature and pattern matching (Figure 2b, see also Figure 3). Finally, the nanostructures are

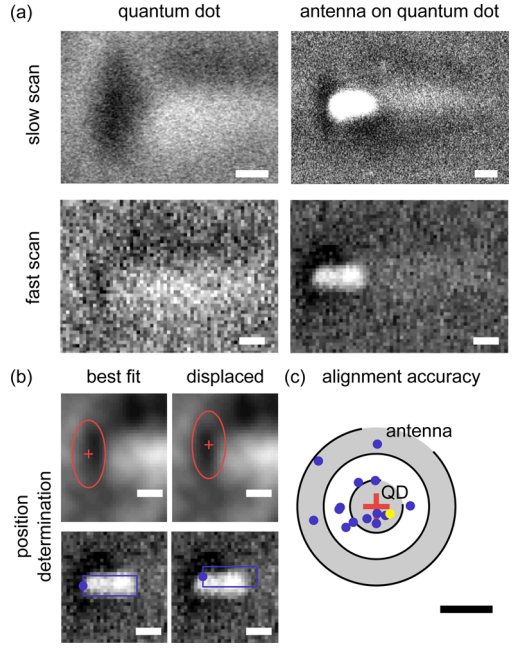

Figure 3. Example of positioning a nanoantenna over a quantum dot. (a) While slow-scan electron micrographs clearly show the topography feature of the quantum dot and the gold antenna, fast-scan images were used for the position determination. (b) An ellipse and a rectangle are used to match the pattern of quantum dot feature and antenna, respectively. The matching is carried out by eye. For determining the position of the quantum dot feature a filtered version of the fast scan image is used (top row). A displacement of 10 nm in horizontal and vertical direction away from the best fitting position is readily visible. (c) Distribution of the positions of nanoantennas with respect to the target quantum dot features. The antenna selected for TEM imaging of the quantum dot (Figure 4) is marked as a yellow dot. 80% of the antennas fall within 15 nm of the target. All scale bars are 20 nm.

fabricated at the desired positions in a second lithography step using the marker grid to align the exposure with respect to the sample (Figure 2c). Also other nanofabrication methods such as focused ion beam milling can be used to fabricate the nanostructures.

We determine the precision of the positioning technique by fabricating 15 gold nanorod antennas aligned to the topography feature corresponding to single quantum dots using electron beam lithography (see Supporting Information for details of sample fabrication). After fabricating the antennas, we determined their positions relative to the marker coordinate system. The in-plane dimensions of the nanorod antennas are about 22 nm × 56 nm. We centered one end of the nanorod on the elliptical topography feature of the quantum dot, which is right above the quantum dot itself (see below). Figure 3a shows

dx.doi.org/10.1021/nl403730q | Nano Lett. 2014, 14, 197−201

scanning electron micrographs of a single plain quantum dot feature and one decorated with an antenna. While slow-scan SEM images clearly show the surface features, it is advisable to reduce the integration time when acquiring images for position controlled fabrication of nanostructures. In this way sample drift during image acquisition as well as sample contamination are minimized. Additionally, a high dose of electrons may degrade the emission properties of the quantum dots. We have verified that fast-scan SEM imaging and electron beam lithography does not harm the emitters (for details see Supporting Information). Typical fast-scan electron micrographs are shown in the second row of Figure 3a. To determine the position of the quantum dot features from such images we first reduce noise by low-pass and Gaussian smoothing filters (Figure 3b). In the filtered image the surface features related to quantum dot and antenna are clearly visible. The position of these features is determined by placing an ellipse and a rectangle on the quantum dot and the antenna, respectively. The size of these shapes is kept constant for the whole data set. The midpoint of the ellipse and the end-point of the rectangle are used to define the positions (marked by a cross and a circle, respectively). The best-fitting position of the shapes was determined by eye. Small displacements in the position of the rectangle or ellipse are readily visible to the eye, as illustrated in Figure 3b, where the matching shape is displaced by 10 nm in both the horizontal and the vertical directions from the position determined as optimal. A displacement of this size results in a clear mismatch between the frame and the SEM feature. This manual method was found to be more robust and as sensitive as a numerical spatial cross correlation method. A detailed comparison between the two methods is presented in the Supporting Information.

Figure 3c shows the distance between the nanoantennas and their target quantum dot feature. For 80% of the structures, the difference between the intended and the actual position is below 15 nm. 50% of the antennas fall within 11 nm, which we take as the accuracy of our positioning method. This shows that our alignment method can be used to fabricate advanced structures with good yield. The remaining spread in the distances is due to three sources: the accuracy in determining positions from the micrographs before and after fabrication of the nanostructures and the alignment of the coordinate systems in the second lithography step. Thus the real alignment precision is better, because the second SEM imaging step leads to additional error due to sample drift. Finally, we remark that the distribution in Figure 3c reflects quantum dots on five SEM micrographs and 11 independent procedures to align sample and lithography coordinate systems. After each alignment we patterned one or two antennas. Our data therefore illustrates the reproducible accuracy of our method and not the performance achievable in the best case.

To confirm the location of the quantum dot with respect to the surface topography feature and nanoantenna we image a thin lamella, which contains the positioned structure of Figure 3b, using cross-section transmission electron microscopy (TEM). The TEM sample was prepared by focused ion beam milling. The selected quantum dot-antenna pair is marked as a yellow dot in Figure 3c. We observe that the quantum dot is located right below the depression in the sample surface (Figure 4). The nanostructure is perfectly aligned with respect to the quantum emitter. Comparing the center of mass of the line scans shown in Figure 4, we determine a lateral deviation of only 2.2 nm for the investigated antenna−quantum dot pair. In

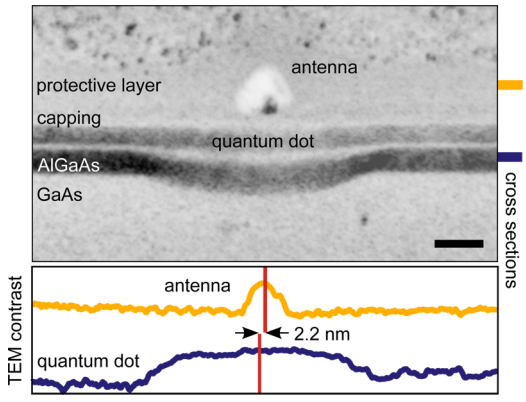

Figure 4. Cross section transmission electron micrograph. The thin lamella has surfaces perpendicular to the long side of the antenna. The positioned antenna (bright) is found centered above the GaAs quantum dot. The quantum dot is formed as thicker part of a thin GaAs layer (bright) between two AlGaAs barrier layers (dark). The image was acquired in dark field mode, using chemically sensitive (002) reflection, and is shown for clarity in a reversed color map. The line scans of the micrograph intensity across the metallic structure and the quantum dot are taken at positions indicated by the colored bars beside the micrograph. The widths of the bars indicate the areas used for generating the line scans.The line scans reveal that the gold nanostructure is almost perfectly centered on the quantum dot. The centers of mass of the line scans, indicated by red lines, differ by only 2.2 nm. The scale bar is 20 nm.

addition to demonstrating the excellent precision of our positioning method, the micrograph shown in Figure 4 is to our knowledge the first TEM micrograph of a strain-free GaAs/AlGaAs quantum dot. This method allows imaging the structural properties of individual preselected nanostructures with subnanometer resolution and correlating such data with results from optical experiments. A random cut through the sample will contain very few if any of such low-density quantum dots. Our positioning method thus also opens up ways to study the structural properties of low-density emitters.

Let us now turn to the antenna's influence on the optical response of the quantum dot. For this we fabricated resonant optical antennas positioned next to the quantum dots. The rectangular gold nanoantennas have in-plane dimensions of 147 nm × 76 nm and are 55 nm thick. The structures were designed so that the transverse plasmon resonance occurred close to the emission wavelength of the emitters (755 nm), while the longitudinal plasmon was off-resonant (see Supporting Information for scattering spectra). Both directions are aligned with the two energetically degenerate in-plane transition dipole moments of the quantum dots. The samples were characterized in a home-built low-temperature confocal laser scanning microscope using continuous wave excitation at 532 nm wavelength, which is off-resonant both with respect to the quantum dot and the nanoantenna. Therefore, the antenna does not influence the excitation process. For off-resonant excitation the exciton states are populated with equal probability,[25] and these states decay independently. Finally, for the excitation powers used in the experiments we have not observed autofluorescence from the antennas on similar samples. Details of the optical properties of the quantum dots as well as of the experimental setup have been published in ref 23.

Figure 5 summarizes the results of the luminescence measurements on the realized antenna-coupled quantum dot

dx.doi.org/10.1021/nl403730q | Nano Lett. 2014, 14, 197−201

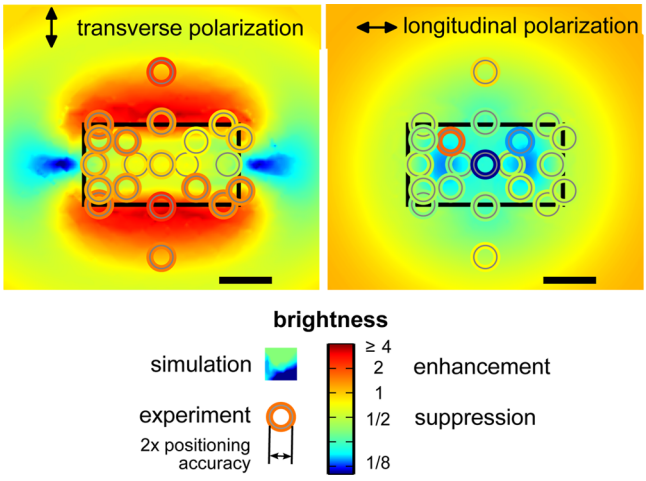

Figure 5. Influence of a resonant antenna on the measured brightness of single quantum dots. As a function of the relative position of quantum dot and optical antenna we find a strong position dependence of the observed brightness of the emitter in numerical simulations (pseudocolor plot) as well as in the experiment (color of the rings): on a length scale of less than 20 nm the collected luminescence changes by more than a factor of 2. Within the accuracy of the positioning procedure (circle radius) we observe good agreement between simulations and experiment. The scale bar is 50 nm.

structures. Due to the lower than unity quantum efficiency of these emitters,[23] a modification of the radiative and nonradiative decay rates is directly visible in the photoluminescence intensity. The photoluminescence intensity in two orthogonally polarized detection channels is normalized to the mean brightness of a reference ensemble of 30 quantum dots without antennas (standard deviation of brightness 14%). The reference ensemble was measured from an area next to the antenna-coupled emitters. The pseudocolor plot shows the results for simulations of the emission collected in the experiment, which take into account the collection solid angle (see details on the simulations in the Supporting Information). The colored rings represent experimental data for different quantum dot positions. As the optical properties of the self-assembled quantum dots and the optical antennas exhibit narrow ensemble distributions, the results for all 21 structures are visualized in one plot. The radius of the ring corresponds to the positioning accuracy of 11 nm. In many cases the color of the ring blends with the simulated image in the background, indicating good agreement between experiment and simulation. Note that the center position of the ring is the designed target position, not a position determined after fabrication. For collected luminescence polarized along the transverse direction the signal is enhanced along the long edges as expected if one approximates the antenna as an oscillating dipole. Similarly, close to the long ends luminescence is suppressed, also in agreement with the dipole model. For collected emission polarized along the longitudinal direction of the antenna we observe suppression for all but one of the quantum dots. This suppression is a consequence of coupling to higher order, nonradiating modes of the antenna which are not visible in far-field scattering. The one emitter that shows a clear enhancement of brightness in the longitudinal polarization direction may be due to an exceptional quantum dot or a defective antenna. In the simulations we find (data not shown) that in general the antenna conserves the emission polarization of the quantum dot. Only for dots close to the corners of the antenna part of radiation ends up in the orthogonal detection channel. The simulations agree with the experiments on the trend in the brightness data but overestimate the suppression under the antenna. This might point to a failure of the point dipole approximation[26] used for the quantum dot in the simulations as the electric field changes significantly over the length scales of our extended quantum emitter (compare Figures 1 and 4).

In conclusion, we have demonstrated a method to fabricate nanostructures with a median 11 nm alignment precision with respect to single GaAs semiconductor quantum dots. This is more precise than all length scales of the optical nearfield and the in-plane dimensions of the quantum dot. Our method allows the nanostructures to be fabricated using state-of-the-art nanofabrication methods such as electron beam lithography and focused ion beam milling. Our positioning technique is fast, reliable, and reproducible and can be automated. As first applications of our method we were able to mark a single quantum dot for selective TEM sample preparation and to image such low-density self-assembled semiconductor quantum dots with TEM, as well as to couple single quantum dots to optical antennas to modify their brightness. The quantum dots used here have a relatively low quantum efficiency[23] resulting in only small changes in the excited state lifetime when coupled to nanoantennas. However, these quantum dots are robust nonblinking single photon sources,[27] and similar emitters have recently been used as light sources in spectroscopy.[28] Optimized near-surface GaAs quantum dots with higher quantum efficiency combined with improved plasmonic structures are thus a promising route to obtain a single photon transistor.[1]

■ ASSOCIATED CONTENT

Ⓢ Supporting Information

Details on sample growth, position determination, scanning electron microscopy, sample fabrication, numerical simulations, scattering properties of antennas and additional references. This material is available free of charge via the Internet at http://pubs.acs.org.

■ AUTHOR INFORMATION

Corresponding Author

*E-mail: markus.lippitz@uni-bayreuth.de.

Present Addresses

(K.L.) Institute of Physical Chemistry, University of Cologne, Luxemburger Strasse 116, D-50939 Köln, Germany.
(M.L.) Experimental Physics III, University of Bayreuth, Universitätsstrasse 30, D-95447 Bayreuth, Germany.

Author Contributions

M.P. and K.L. contributed equally.

Notes

The authors declare no competing financial interest.

■ ACKNOWLEDGMENTS

The authors acknowledge funding from DFG (research group FOR730) and the Academy of Finland (project 252421).

■ REFERENCES

(1) Chang, D. E.; Sørensen, A. S.; Demler, E. A.; Lukin, M. D. *Nat. Phys.* **2007**, *3*, 807−812.
(2) Orrit, M. *Nat. Phys.* **2007**, *3*, 755−756.
(3) Benson, O. *Nature* **2011**, *480*, 193−199.

(4) Schuller, J. A.; Barnard, E. S.; Cai, W.; Jun, Y. C.; White, J. S.; Brongersma, M. L. *Nat. Mater.* **2010**, *9*, 193−204.
(5) Novotny, L.; van Hulst, N. *Nat. Photonics* **2011**, *5*, 83−90.
(6) Reithmaier, J. P.; Sek, G.; Loffler, A.; Hofmann, C.; Kuhn, S.; Reitzenstein, S.; Keldysh, L. V.; Kulakovskii, V. D.; Reinecke, T. L.; Forchel, A. *Nature* **2004**, *432*, 197−200.
(7) Englund, D.; Majumdar, A.; Bajcsy, M.; Faraon, A.; Petroff, P.; Vučković, J. *Phys. Rev. Lett.* **2012**, *108*, 093604.
(8) Reinhard, A.; Volz, T.; Winger, M.; Badolato, A.; Hennessy, K. J.; Hu, E. L.; Imamoglu, A. *Nat. Photonics* **2012**, *6*, 93−96.
(9) Farahani, J. N.; Pohl, D. W.; Eisler, H.-J.; Hecht, B. *Phys. Rev. Lett.* **2005**, *95*, 017402.
(10) Anger, P.; Bharadwaj, P.; Novotny, L. *Phys. Rev. Lett.* **2006**, *96*, 11302.
(11) Kühn, S.; Hakanson, U.; Rogobete, L.; Sandoghar, V. *Phys. Rev. Lett.* **2006**, *97*, 017402.
(12) Kinkhabwala, A.; Yu, Z.; Fan, S.; Avlasevich, Y.; Müllen, K.; Moerner, W. E. *Nat. Photonics* **2009**, *3*, 654−657.
(13) Curto, A. G.; Volpe, G.; Taminiau, T. H.; Kreuzer, M. P.; Quidant, R.; van Hulst, N. F. *Science* **2010**, *329*, 930−933.
(14) Bharadwaj, P.; Novotny, L. *Opt. Express* **2007**, *15*, 14266−14274.
(15) Tam, F.; Goodrich, G. P.; Johnson, B. R.; Halas, N. J. *Nano Lett.* **2007**, *7*, 496−501.
(16) Ringler, M.; Schwemer, A.; Wunderlich, M.; Nichtl, A.; Kurzinger, K.; Klar, T. A.; Feldmann, J. *Phys. Rev. Lett.* **2008**, *100*, 203002.
(17) Bek, A.; Jansen, R.; Ringler, M.; Mayilo, S.; Klar, T. A.; Feldmann, J. *Nano Lett.* **2008**, *8*, 485−490.
(18) Schietinger, S.; Barth, M.; Aichele, T.; Benson, O. *Nano Lett.* **2009**, *9*, 1694−1698.
(19) Badolato, A.; Hennessy, K.; Atature, M.; Dreiser, J.; Hu, E.; Petroff, P. M.; Imamoglu, A. *Science* **2005**, *308*, 1158−1161.
(20) Schneider, C.; Strauß, M.; Sünner, T.; Huggenberger, A.; Wiener, D.; Reitzenstein, S.; Kamp, M.; Höfling, S.; Forchel, A. *Appl. Phys. Lett.* **2008**, *92*, 183101.
(21) Dousse, A.; Lanco, L.; Suffcynski, J.; Semenova, E.; Miard, A.; Lematre, A.; Sagnes, I.; Roblin, C.; Bloch, J.; Senellart, P. *Phys. Rev. Lett.* **2008**, *101*, 267404.
(22) Thon, S. M.; Rakher, M. T.; Kim, H.; Gudat, J.; Irvine, W. T. M.; Petroff, P. M.; Bouwmeester, D. *Appl. Phys. Lett.* **2009**, *94*, 111115.
(23) Pfeiffer, M.; Lindfors, K.; Wolpert, C.; Atkinson, P.; Benyoucef, M.; Rastelli, A.; Schmidt, O. G.; Giessen, H.; Lippitz, M. *Nano Lett.* **2010**, *10*, 4555−4558.
(24) Atkinson, P.; Zallo, E.; Schmidt, O. G. *J. Appl. Phys.* **2012**, *112*, 054303.
(25) Pfeiffer, M.; Lindfors, K.; Atkinson, P.; Rastelli, A.; Schmidt, O. G.; Giessen, H.; Lippitz, M. *Phys. Status Solidi B* **2011**, *249*, 678−686.
(26) Andersen, M. L.; Stobbe, S.; Sørensen, A. S.; Lodahl, P. *Nat. Phys.* **2011**, *7*, 215−218.
(27) Kumar, S.; Trotta, R.; Zallo, E.; Plumhof, J. D.; Atkinson, P.; Rastelli, A.; Schmidt, O. G. *Appl. Phys. Lett.* **2011**, *99*, 161118.
(28) Akopian, N.; Wang, L.; Rastelli, A.; Schmidt, O. G.; Zwiller, V. *Nat. Photonics* **2011**, *5*, 230−233.

dx.doi.org/10.1021/nl403730q | *Nano Lett.* 2014, 14, 197−201